Quorum-sensing regulation governs bacterial adhesion, biofilm development, and host colonization in Pantoea stewartii subspecies stewartii

Maria D. Koutsoudis, Dimitrios Tsaltas, Timothy D. Minogue, and Susanne B. von Bodman

PNAS 2006;103;5983-5988; originally published online Apr 3, 2006;
doi:10.1073/pnas.0509860103

Quorum-sensing regulation governs bacterial adhesion, biofilm development, and host colonization in *Pantoea stewartii* subspecies *stewartii*

Maria D. Koutsoudis*†, Dimitrios Tsaltas†‡, Timothy D. Minogue‡§, and Susanne B. von Bodman*‡¶

Departments of *Molecular and Cell Biology and ‡Plant Science, University of Connecticut, Storrs, CT 06269; and §Pathogen Functional Genomic Resource Center, Center for Genomic Research, 9712 Medical Drive, Rockville, MD 20850

Edited by Luis Sequeira, University of Wisconsin, Madison, WI, and approved February 2, 2006 (received for review November 14, 2005)

The phytopathogenic bacterium *Pantoea stewartii* subsp. *stewartii* synthesizes stewartan exo/capsular polysaccharide (EPS) in a cell density-dependent manner governed by the EsaI/EsaR quorum-sensing (QS) system. This study analyzes biofilm development and host colonization of the WT and QS regulatory mutant strains of *P. stewartii*. First, we show that the cell density-dependent synthesis of stewartan EPS, governed by the EsaI/EsaR QS system, is required for proper bacterial adhesion and development of spatially defined, 3D biofilms. Second, a nonvirulent mutant lacking the *esaI* gene adheres strongly to surfaces and develops densely packed, less structurally defined biofilms *in vitro*. This strain appears to be arrested in a low cell density developmental mode. Exposure of this strain to exogenous *N*-acyl-homoserine lactone counteracts this adhesion phenotype. Third, QS mutants lacking the EsaR repressor attach poorly to surfaces and form amorphous biofilms heavily enmeshed in excess EPS. Fourth, the WT strain disseminates efficiently within the xylem, primarily in a basipetal direction. In contrast, the two QS mutant strains remain largely localized at the site of infection. Fifth, and most significantly, epifluorescence microscopic imaging of infected leaf tissue and excised xylem vessels reveals that the bacteria colonize the xylem with unexpected specificity, particularly toward the annular rings and spiral secondary wall thickenings of protoxylem, as opposed to indiscriminate growth to fill the xylem lumen. These observations are significant to bacterial plant pathogenesis in general and may reveal targets for disease control.

maize | xylem | pathogenesis | dissemination

The recent research emphasis in bacterial cell–cell communication (1–5) and microbial biofilms (6–9) has reinforced the concept that bacteria are social organisms that exist as multicellular entities in nature. Multicellular bacterial development and morphogenesis is well described in species of *Myxobacterium*, *Caulobacter*, and *Bacillus* (10–12), and similar, though perhaps less dramatic, coordinate behaviors exist in many other bacteria. Bacteria that grow in natural habitats generally transition through repetitive cycles of differentiation from free-swimming planktonic bacteria to complex, organized, surface-adherent communities (6, 9, 13–15). Such developmental cycles are governed by complex, integrated regulatory networks, which respond to a continuum of environmental and metabolic inputs. Quorum-sensing (QS) regulation is a central component within a number of bacterial regulatory hierarchies (16). It enables bacteria to monitor their own population density by means of small, diffusible signals and to synchronize the expression of specialized gene systems with cell density (17). As such, QS systems can serve as switching mechanisms between successive phases of bacterial development. The most studied QS signaling systems involve membrane-permeable *N*-acyl-L-homoserine lactones (AHLs) in Gram-negative bacteria and linear or cyclic oligopeptides in Gram-positive bacteria (1, 2, 5). Both bacterial groups frequently produce a second class of furanone-based QS signals that are implicated in interspecies-specific communication (18). Many bacteria depend on QS regulated gene systems to establish symbiotic or pathogenic interactions with eukaryotic hosts or to colonize inanimate natural habitats (8, 19–25). It is also recognized as a key mechanism for governing various aspects of biofilm development, including adhesion, motility, maturation, and dispersion (7, 9, 26, 27). This realization, coupled with the fact that bacterial biofilms are frequently associated with bacterial infections, contamination of foods, and corrosion of industrial and public infrastructure, has prompted considerable interest in the use of QS signal degradative measures or chemical inhibitors to contain harmful bacterial biofilms (28, 29).

Our interest in studying the biofilm characteristics of *Pantoea stewartii* derives from the observation that QS regulatory mutants of this organism are severely restricted in causing Stewart's vascular wilt and leaf blight in sweet corn and maize (30). This disease generally initiates when infected corn flea beetles feed on the host plant and deposit a bacterial inoculum directly into the feeding wounds (31, 32). The bacteria subsequently colonize the xylem vessels, where their production of large amounts of bacterial exo/capsular polysaccharide (EPS), also termed stewartan, blocks the free flow of water, leading to the wilting condition (33, 34). We have shown in previous studies that *P. stewartii* utilizes the EsaI/EsaR QS regulatory system to govern the cell density-dependent expression of the well characterized *cps* gene system that encodes the structural functions for EPS synthesis (30, 35). EsaI is a typical AHL signal synthase that catalyzes the preferential synthesis of *N*-3-oxo-hexanoyl homoserine lactone (35, 36). EsaR is a homologue of LuxR but differs from the paradigm by functioning as a repressor of transcription at low cell density or in the absence of the QS signal (30, 35, 37, 38). Derepression of such EsaR-regulated genes requires inducing levels of the AHL coinducer (37, 38). A mutant (ESN51) lacking the *esaI* gene is repressed for EPS synthesis and is therefore avirulent (30, 35). In contrast, strains mutated in the *esaR* gene (ESΔR and ESΔIR) produce high levels of EPS constitutively. Surprisingly, these hypermucoid mutant strains are also significantly attenuated in their ability to cause Stewart's wilt disease, even though they synthesize an abundance of the EPS virulence factor (30).

The realization that the lack of, or the premature synthesis of, EPS interferes with the normal disease process prompted the consideration that Stewart's wilt infections may rely on the

Conflict of interest statement: No conflicts declared.

This paper was submitted directly (Track II) to the PNAS office.

Abbreviations: AHL, acyl-L-homoserine lactone; QS, quorum-sensing; EPS, exo/capsular polysaccharide; CV, crystal violet.

†M.D.K. and D.T. contributed equally to this work.

¶To whom correspondence should be addressed at: Department of Plant Science, University of Connecticut, 302 ABL, 1390 Storrs Road, Storrs, CT 06269-4163. E-mail: susanne.vonbodman@uconn.edu.

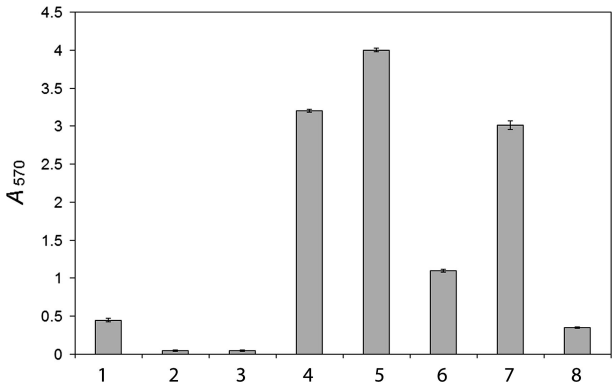

Fig. 1. Adhesion of *P. stewartii* WT and EPS- and QS-deficient mutant strains. The level of CV stain retained, measured spectrophotometrically (A_{570}), reflects the mass of adherent cells. Strains assayed, shown on the *x* axis, were as follows: 1, DC283 (WT); 2, ESΔR (*esaR*); 3, ESΔIR (*esaI*/*esaR*); 4, ESN51 (*esaI*); 5, DM223 (*wceG*); 6, DM220 (*wceL*); 7, Gal8 (Δ*cps*); 8, Gal8 (pES2144). Vertical bars represent the standard error from the mean.

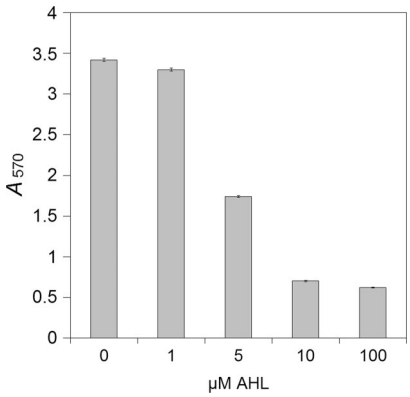

Fig. 2. AHL counteracts the mutant adhesion phenotype of strain ESN51. The AHL-deficient QS mutant strain ESN51 was grown in the absence and presence of increasing levels of exogenous *N*-3-oxo-hexanoyl homoserine lactone. Adhesion was measured by CV staining as before. Vertical bars represent the standard error from the mean.

temporal expression of functions normally associated with bacterial development. We reasoned that the out-of-phase synthesis of EPS might hamper, or interfere with the expression of, functions typically expressed during the early phases of bacterial development and infection. Bacterial adhesion has been implicated as an important step in initiating bacterial parasitic and symbiotic plant–microbe interactions for >20 years (39–41). The data presented in this report are consistent with these predictions showing that the QS controlled timing and level of EPS produced greatly influence the degree of bacterial adhesion during *in vitro* biofilm formation and dissemination within the plant host. Therefore, we suggest a functional corollary between bacterial biofilm development and xylem colonization similar to that described for *Xylella fastidiosa* infections of grape vine and *Clavibacter michiganensis* subsp. *sepedonicus* of potato (42–47). Most significantly, our microscopic studies show that *P. stewartii* colonizes the xylem of corn with spatial specificity rather than by indiscriminate growth to fill the lumen of the xylem. Together, our findings underscore the importance of studying bacterial plant infection processes in terms of temporally defined developmental steps to gain a deeper appreciation of disease mechanisms and to identify targets for disease control. In this context, plants engineered to synthesize QS signals can suppress plant diseases, presumably by disrupting the spatiotemporal regulation of important virulence processes (22, 48–50).

Results

Influence of QS on *in Vitro* Surface Adhesion. The coordinate cell density-dependent synthesis of EPS in *P. stewartii*, governed by QS regulation, is critical for normal Stewart's wilt disease development (30). It follows that delayed EPS synthesis might enable the bacteria to attach to a surface and/or transition through the early steps of biofilm development. To test this prediction, we conducted *in vitro* adhesion assays in poly(vinyl chloride) (PVC) microtiter dishes containing LB-glucose medium. This assay used a 12-h growth period and spectrophotometric determination of cell density (OD_{600}), followed by removal of the planktonic cell fraction and crystal violet (CV) staining of the remaining attached cells. Solubilization of the CV stain by addition of ethanol provides an indirect, quantitative measure of the adherent cell mass within a given well. The data summarized in Fig. 1 show that the WT strain, DC283 (*esaI*$^+$, *esaR*$^+$, EPS$^+$), adheres at low but significant levels to the PVC surface. The AHL-deficient strain ESN51 (*esaI*$^-$, *esaR*$^+$, EPS$^-$) attaches proficiently, with 10-fold higher levels of CV stain retained by this strain. In contrast, the hypermucoid mutant strains ESΔR (*esaI*$^+$, *esaR*$^-$, EPS^{+++}) and ESΔIR (*esaI*$^-$, *esaR*$^-$, EPS^{+++}) retain only basal levels of CV, similar to the negative medium control, indicating a general lack of adhesion.

Bacterial Adhesion Is Inversely Proportional to the Concentration of Synthetic *N*-3-oxo-hexanoyl Homoserine Lactone Provided. The *esaI* mutant strain ESN51 lacks the ability to synthesize AHL. Thus, the strong adhesion characteristics of this strain should be counteracted by the addition of exogenous AHL. The data graphically summarized in Fig. 2 show a clear inverse relationship between bacterial adhesion based on CV stain retention and the concentrations of exogenous AHL included in the growth medium. In fact, the addition of 10 μM AHL, which corresponds to the physiological AHL-inducing levels for *P. stewartii* (30), significantly relieves the strong adhesion phenotype. It is important to note that AHL promotes a reduction in adhesion, whether present throughout growth (Fig. 2) or added 1 and 4 h after inoculation (data not shown), suggesting that adhesion may be a transient feature of bacterial development.

Adhesion Properties of EPS-Deficient Mutant Strains. Strain ESN51 is highly adhesion-proficient, whereas the constitutively EPS-expressing strains ESΔR and ESΔIR are adhesion-deficient (Fig. 1), suggesting that EPS present during early growth (low cell density) interferes with cellular adhesion. This prediction was tested by adhesion assays using structural EPS biosynthetic mutant derivatives of WT strain DC283. The structural genes are in the well defined *cps* biosynthetic locus (37, 51). Such EPS mutant strains should exhibit the same strong adhesion phenotype as strain ESN51. The graphic summary of Fig. 1 shows that the EPS-deficient mutants DM220, lacking the essential WceL glycosyl transferase function, and Gal8, lacking the entire *cps* gene cluster (37, 51, 52), exhibit the same robust adhesion phenotype as strain ESN51. The *cps* operon expressed in trans from plasmid pES2144 restores low WT-level adhesion to Gal8. Mutant strain DM223 (*wceG*$^-$), with an intermediary EPS phenotype (37, 51, 52), exhibits midlevel adhesion.

Loss of Adhesion in ESΔIR *cps* Structural Mutant Backgrounds. The above data suggested that the amount and timing of EPS production have dramatic effects on *P. stewartii* surface adhesion, suggesting that the EPS creates a physical barrier between the bacterial adhesion factors and a given substrate. However, one cannot ignore the possibility that adhesion and EPS synthesis are subject to coordinate, inverse regulation. We tested this

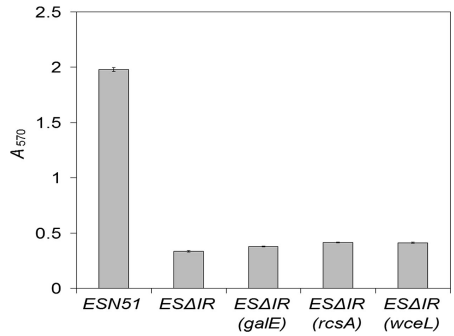

Fig. 3. Adhesion depends on the presence of the EsaR QS regulator. ESΔIR mutant strains with genetic defects in *galE*, *wceL*, or *rcsA* are nonmucoid, similar to strain ESN51. These triple mutant strains are adhesion-deficient, in stark contrast to strain ESN51. Vertical bars represent the standard error from the mean.

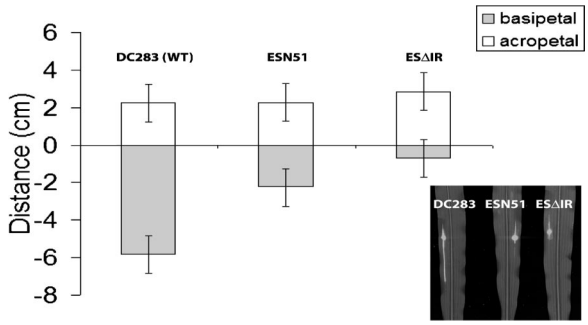

Fig. 5. Dissemination of *P. stewartii* WT and QS mutant strains in seedling leaves of the susceptible sweet corn cv. Jubilee. Dissemination was measured in cm from the point of inoculation and ending where *gfp*-expressing cells are no longer detected. (*Inset*) Visualization of bacterial movement by PhosphorImaging.

possibility with a set of three EPS-deficient mutant strains created in the otherwise hypermucoid, nonadherent ESΔIR (*esaI*$^-$, *esaR*$^-$, EPS^{+++}) parent strain (37). We reasoned that if the presence of EPS merely masks the surface-exposed adhesion factors, then the nonmucoid derivatives of ESΔIR should adhere to the same degree as the EPS mutant strains Gal8 and DM220 and the AHL-deficient strain ESN51. The data summarized in Fig. 3 show that the EPS-deficient triple mutants ESΔIR*galE*, ESΔIR*rcsA*, and ESΔIR*wceL*, lacking a UDP-glucose-4-epimerase, the RcsA activator of *cps* genes, and a glycosyl transferase, respectively (37, 51, 52), all exhibit limited adhesion, arguing against a mere EPS masking effect.

The Role of QS in *in Vitro* Biofilm Formation. The aberrant adhesion phenotypes of the QS mutant strains ESΔIR (minimal adhesion) and ESN51 (strong adhesion) should also affect biofilm development by *P. stewartii*. Therefore, we examined the *in vitro* biofilm characteristics of GFP-tagged WT and QS mutant strains grown on borosilicate glass coverslips and visualized by epifluorescence and confocal laser scanning microscopy (CLSM) (Fig. 4). Fig. 4 *A* and *B* represent a top-down (*xy*) view of bacterial biofilms developed after 12 and 24 h of growth, respectively. The GFP-tagged WT strain, DC283-GFP, organizes into distinctive microcolonies after 12 h, which develop into more densely populated biofilms (Fig. 4*B*) separated by distinct regions of voids after 24 h of growth (Fig. 4*B Inset*). In contrast, strain ESN51-GFP forms numerous smaller bacterial aggregates distributed across the glass surface after 12 h and a compact, less spatially defined biofilm after 24 h of growth. The hypermucoid strain ESΔIR-GFP develops small, heavily matrix-encased microcolonies after 12 h and a mat of amorphous biofilm after 24 h of growth. The ESΔIR biofilms dislodged readily from the borosilicate glass substrate during manipulation and gentle rinsing (data not shown). Fig. 4*C* shows the 3D (*xyz*) rendering of serial horizontal (*xy*) CLSM scans taken of the biofilm displayed in Fig. 4*B*. The WT GFP-tagged strain develops a dramatic biofilm architecture typified by distinct 3D towers (broad at the base) that are separated by regions of voids. In contrast, strain ESN51-GFP forms tightly packed bacterial mats and gives rise to occasional, thin vertical spikes of bacterial chains. The hypermucoid strain ESΔIR-GFP produces confluent, loosely attached biofilms devoid of pronounced 3D architecture.

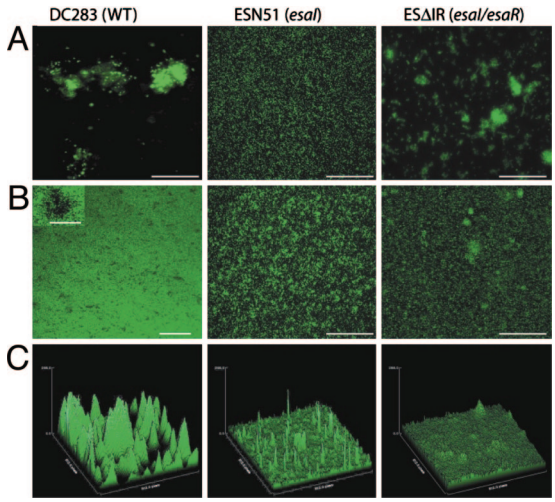

Fig. 4. *In vitro* biofilm characteristics of GFP-tagged WT and QS mutant strains. Biofilms were grown in LB (glucose) on borosilicate coverslips and observed by epifluorescence microscopy after 12-h incubation (*A*) and by confocal laser scanning microscopy after 24-h incubation [top-down view (*xy*)] (*B*). *C* shows a 3D (*xyz*) rendering of the 24-h biofilms. (Scale bars, 50 μm in *A–C* and 20 μm in *Inset*.)

The Role of QS Regulation During Plant Infection. Our previous studies showing that the QS mutant strains are significantly less virulent was based on a subjective disease rating scale (30). Here, we wished to examine the dissemination of the GFP-tagged *P. stewartii* strains in real time by epifluorescence microscopy and PhosphorImaging. The GFP-tagged strains used in this assay have *in vitro* growth rates similar to those of the untagged parent strains (data not shown). Graphically summarized and visually illustrated in Fig. 5, strain DC283-GFP moves efficiently within the xylem and disseminates preferentially in a basipetal direction. In contrast, the strongly adherent strain, ESN51-GFP, and the hypermucoid strain ESΔIR-GFP show greatly reduced basipetal movement within the same time frame. All strains disperse to approximately the same degree in an acropetal direction.

Epifluorescence Imaging of Colonization Patterns of Inoculated Xylem Vessels. Epifluorescence imaging of intact leaves provided some hints that the bacteria colonize the xylem vessel in a distinct pattern (Fig. 6*A*, epifluorescence image; Fig. 6*B*, bright field, uninoculated). Therefore, we examined inoculated median veins by carefully dissecting and tweezing out individual vessels. Bright-field microscopy resolves the structural details of a xylem vessel with clear definition of the annular rings (Fig. 6*C*). The epifluorescence images of infected xylem are striking. Specifically, the WT DC283-GFP (Fig. 6*D*) and the highly adhesion-

MICROBIOLOGY

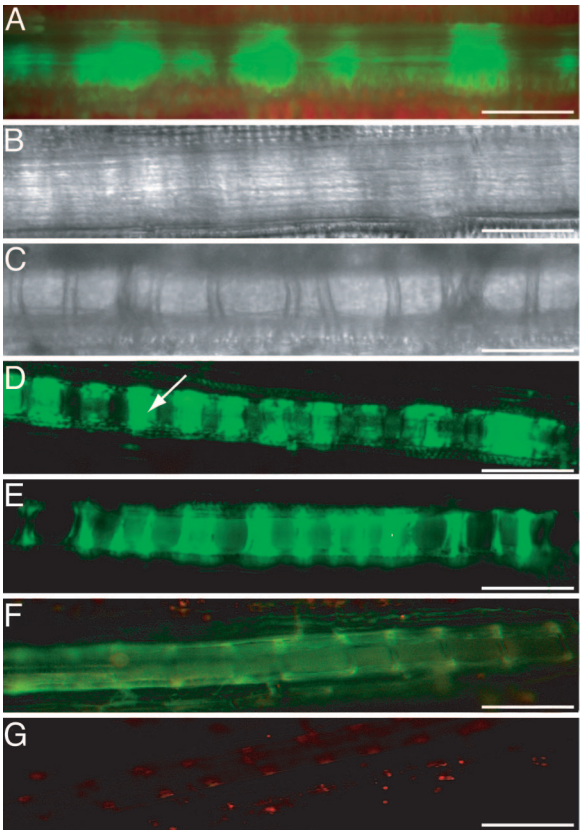

Fig. 6. Xylem colonization by GFP-tagged *P. stewartii*. (*A* and *B*) Patterned xylem colonization observed by epifluorescence microscopy of intact leaf tissue (*A*) compared with an uninoculated vessel of intact leaf tissue observed by bright-field microscopy (*B*). (*C*) Bright-field image of an uninoculated excised xylem vessel clearly resolving the annular rings. (*D–G*) Epifluorescence images of excised vessels infected with WT strain DC283-GFP (arrow indicates a colonized ring) (*D*), mutant strain ESN51-GFP (*E*), hypermucoid strain ESΔIR-GFP (*F*), and uninfected (*G*). The colonization pattern shown is typical for all samples examined. (Scale bars, 75 μm.)

proficient ESN51-GFP bacteria (Fig. 6*E*) exhibit a definite tendency to colonize the annular ring structures. In contrast, the adhesion-deficient hypermucoid strain ESΔIR-GFP lacks such specificity with the bacteria diffusely distributed within the xylem lumen (Fig. 6*F*). Uninoculated xylem (Fig. 6*G*) shows only low-level autofluorescence. Colonization specificity is also evident in xylem with spiral wall thickenings (data not shown). Moreover, the bacteria appear to colonize thin, parallel, longitudinal structures distributed over the inner face of the xylem vessels, giving the impression of a "striped" colonization pattern (Fig. 6*A*).

Scanning Electron Microscopy of Infected Maize Xylem. We also examined transverse sections of infected leaves by scanning electron microscopy. The images of Fig. 7 show that the WT strain DC283 forms 3D structures reminiscent of multicellular aggregates or biofilms seen under *in vitro* growth. The WT aggregates appear to be tightly attached to the xylem wall in specific places as shown in the image of Fig. 7*A*, which also reveals the development of tower-like, 3D structures composed of EPS-encased bacteria developing from a foundation of adherent cells. These towers meet roughly in the center of the xylem lumen where they fuse. Fig. 7*B* shows a more developed WT biofilm composed of larger numbers of heavily EPS-enmeshed bacterial cells. A xylem vessel infected with the AHL-deficient, EPS-repressed strain ESN51 (Fig. 7*C*) shows

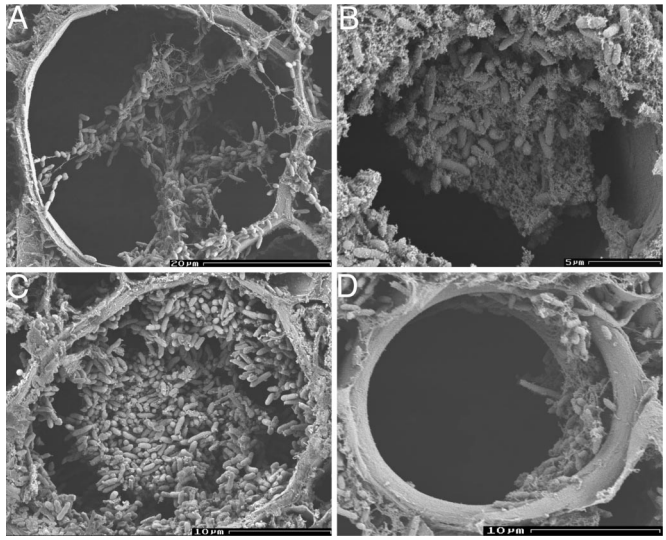

Fig. 7. Infected xylem vessels of sweet corn leaves visualized by scanning electron microscopy. (*A* and *B*) WT strain DC283. (*C*) Mutant strain ESN51. (*D*) Mutant strain ESΔIR. The images are cross sections of infected xylem and are representative of the observations made from two experiments with three replicates each. (Scale bars, 5 μm in *A–C* and 10 μm in *D*.)

tightly packed, adherent bacteria lacking any EPS fibril material. However, individual cells appear interconnected by undefined bacterial appendages. Lastly, and in contrast, the hypermucoid strain ESΔIR appears to develop less densely populated cellular masses that are heavily enmeshed in EPS (Fig. 7*D*). These bacterial agglomerates are invariably collapsed to one side of the xylem, presumably because they lack the structural support of adherent biofilms.

Discussion

The results presented here establish the biological role and significance of the cell density-dependent synthesis of stewartan EPS by *P. stewartii* in effective host colonization. The experimental evidence shows that attenuated *in vivo* virulence in the QS regulatory mutant strains ESN51, ESΔR, and ESΔIR correlates with defects in bacterial adhesion. The WT strain, which is repressed for EPS synthesis at low cell density, exhibits low-level, presumably transient adhesion as part of an overall dynamic developmental process. In contrast, the AHL-deficient strain ESN51 displays an unusually robust adhesion phenotype that can be counteracted by exposing surface-adherent bacteria to AHL. This observation suggests that strain ESN51 is developmentally locked into the adhesion phase of biofilm development yet maintains normal clonal growth. Thus, strain ESN51 is capable of forming dense bacterial mats *in vitro* and tightly packed bacterial agglomerates in the *in vivo* xylem vessel. This strain is also able to grow vertically, forming thin spikes of interconnected bacterial chains that project above the bacterial mat. The compact nature of the ESN51 biofilm resembles those of *Escherichia coli* strains defective in colanic acid synthesis and of AHL-deficient *Pseudomonas aeruginosa* strains (13, 53). In contrast, the hypermucoid QS mutant ESΔIR lacks the ability to adhere appreciably to inert surfaces but is able to form amorphous, detached ("floating") biofilms. This strain appears to be locked into a high cell density mode. Accordingly, the inability by all QS regulatory mutant strains to cycle through normal programmed bacterial development leads to the formation of atypical biofilms *in vitro* and loss of dissemination and infectivity *in vivo*.

Our data further suggest that surface adhesion and EPS synthesis may be governed by inverse coordinate regulation. This prediction derives from the observation that the ESΔIR EPS-deficient strains exhibit the same low adhesion phenotype as the hypermucoid parent strain, arguing against a mere masking of adhesion properties by EPS. Also, all adhesion-proficient genotypes tested contain a functional copy of *esaR*, whereas all adhesion-deficient strains tested lack *esaR*. It is possible that EsaR activates the expression of adhesion factor(s) at low cell density. We previously established that EsaR is DNA-binding-competent in the absence of the AHL coinducer and neutralized for DNA binding in the presence of inducing levels of AHL (37, 38). In addition, EsaR can function as a transcriptional activator if a properly spaced EsaR-binding site precedes the regulated promoter (54).

The plant studies presented in this report provide several important insights into how *P. stewartii* colonizes the xylem of maize. Specifically, we show that the WT strain DC283 is extremely efficient in colonizing artificially inoculated xylem vessels, whereas the two QS mutant strains ESN51 and ESΔIR remain largely localized at the site of inoculation. Moreover, the WT strain exhibits a pronounced tendency to disseminate in a basipetal direction, which means that active colonization proceeds against the flow of the xylem fluid. Basipetal colonization of host xylem was reported originally for *Erwinia amylovora* in the xylem colonization of apple seedlings (55) and more recently for *Xylella fastidiosa* during infections of grape vine (46). Both the WT and mutant strains of *P. stewartii* exhibit limited acropetal movement, which may result from negative hydrostatic pressure generated by the incision during manual inoculation. This hypothesis is supported by the observed limited passive movement of fluorescent latex beads within cavitated xylem (46). Cavitation-induced passive bacterial movement may be biologically relevant for *P. stewartii* to gain rapid access into the xylem after deposition by the biological vector, the infected corn flea beetle. Additionally, the epifluorescence microscopic studies reveal that *P. stewartii* colonizes the xylem with a striking degree of spatial specificity instead of indeterminate growth to fill the xylem lumen. One can infer from the images shown in Fig. 6 that the bacteria preferentially colonize the annular and spiral secondary wall thickenings of xylem. Plant xylem consists of two anatomically distinct xylem vessels, the protoxylem (PX), characterized by annular and spiral secondary wall thickenings, and the metaxylem (MX), featuring reticulate and pitted thickenings. Our preliminary assessment suggests that the bacteria preferentially colonize PX, although we have seen the occasional colonization of the bordered pits of MX. These colonization characteristics will prove useful in further delineating the xylem components that mediate the specific bacterial/xylem interactions. Lastly, the scanning electron microscopy analyses of transverse xylem sections clearly show a biofilm-type habit by *P. stewartii* within the host xylem, and the observed *in vivo* biofilm characteristics correlate well with those of *in vitro* biofilms. Specifically, the WT strain appears to be attached at specific sites to the xylem wall, forming a basal layer of adherent cells, which give rise to EPS enmeshed tower-like 3D biofilm structures fused at the center and poised within the lumen of the xylem vessel. The AHL-deficient strain ESN51 forms a densely packed biofilm lacking EPS fibrils, whereas the hypermucoid strain ESΔIR produces structurally weak, amorphous, EPS-encased biofilms that appear collapsed, possibly as a result of critical point drying.

In summary, our data offer important insights into the biological role of QS regulation as a means to facilitate normal, effective colonization of maize xylem by the plant pathogenic bacterium *P. stewartii*. Most significantly, we provide evidence that *P. stewartii*, and possibly other vascular pathogens, display a subcellular specificity for yet unidentified molecular constituents of xylem. Accordingly, our research offers a unique perspective on a previously unrecognized bacterial plant infection strategy and specificity.

Table 1. Strains and plasmids

Strain or plasmid	Relevant genotype	Reference
P. stewartii		
DC283	WT, *Nal*^{R}	51
ESΔIR	Δ(*esaI, esaR*), *Nal*^{R}, *Km*^{R}	35
ESΔR	Δ(*esaI*), *Nal*^{R}, *Cm*^{R}	35
ESN51	*esaI*::Tn*5*seqN51, *Nal*^{R}, *Km*^{R}	35
DM220	Δ*wceG*, *Nal*^{R}, *Km*^{R}	51
DM223	Δ*wceL*, *Nal*^{R}	51
Gal8	Δ(*wceG-galE*), *Nal*^{R}	51
ESΔIR*wceL*	*wceL*::Tn*5gfp-nptII*	37
ESΔIR*rcsA*	*rcsA*::Tn*5gfp-nptII*	37
ESΔIR*galE*	*galE*::Tn*5gfp-nptII*	37
E. coli		
S17-1	RP4 Mob$^+$	35
Plasmids		
pHC60	Broad host range vector carrying *gfp*, *Cm*^{R}	57
pES2144	Genomic clone (*wceG-galE*), *Tc*^{R}	51

Ap^R, ampicillin; *Cm*^{R}, chloramphenicol; *Km*^{R}, kanamycin; *Nal*^{R}, nalidixic acid; *R*, resistance.

Materials and Methods

Bacterial Strains, Growth Conditions, and DNA Techniques. The *E. coli* strain S17-1 was used for conjugal transfer of pHC60 GFP plasmid into *P. stewartii* strains (37, 57). The *P. stewartii* strains were grown at 28°C in LB in the presence of 30 mg/ml nalidixic acid on nutrient agar plates or AB minimal medium [containing (per liter) 3 g of K_2HP0_4, 1 g of NaH_2PO_4, 1 g of NH_4Cl, 0.3 g of $MgSO_4$–$7H_2O$, 0.15 g of KCl, 0.01 g of $CaCl_2$, 2.5 mg of $FeSO_4{\cdot}7H_2O$, and 0.2% glucose] (37). All relevant strains and plasmids are listed in Table 1. DNA techniques were performed by standard methods as described in refs. 30, 35, and 37.

Adhesion Assays. Adhesion was measured by using a poly(vinyl chloride) 96-well plate (Falcon 353913, Becton Dickinson) assay system following the procedure described by O'Toole and Kolter (56). All strains were grown in LB containing 0.2% glucose to an OD_{570} of 0.16. Bacterial adhesion was measured after repetitive washing of the plates and staining with 1% CV for 15 min at room temperature. Excess stain was removed by washing under running tap water, and the CV stain was solubilized by the addition of 150-μl volumes of 95% ethanol added to each well. CV was quantified with a microplate reader at A_{570} absorption wavelength. The values for the quantification of CV staining reported for each strain are the averages generated from growth in 96 wells (one plate) repeated at least six times.

Adhesion Assays in the Presence of AHL. Surface adhesion of strain ESN51 was performed as described. The growth medium was amended with increasing concentrations of AHL ranging from 0 to 100 μM synthetic *N*-3-oxo-hexanoyl homoserine lactone (K3007; Sigma).

Static *in Vitro* Biofilm Assays. Each strain was transformed with plasmid pHC60 expressing a red-shifted GFP (GFP_{S65T}) (57). The *gfp*-expressing bacterial strains were grown overnight on nutrient agar plates at 28°C. Cells were resuspended in LB containing the appropriate antibiotics and grown to midexponential growth phase ($OD_{600} \approx 0.6$), harvested, washed three times with PBS, and resuspended to an OD_{600} of 0.05 into LB supplemented with 0.2% glucose. These cultures were allowed to incubate in 50-ml Falcon tubes (352070; Fisher) in the presence

of borosilicate coverslips (12-540B; Fisher). The coverslips were gently rinsed in water with the exception of those exposed to strain ESΔIR. Bacterial growth was examined with an IX70 microscope (Olympus, Melville, NY) equipped with an S99806 MagnaFire charge-coupled device camera. For confocal laser scanning microscopy, bacterial growth on the coverslips was examined with a TCS SP2 inverted confocal microscope (Leica, Deerfield, IL) to collect *xyz* sections through the biofilm of interest by using a 488-nm laser line excitation wavelength. In each case, a series of images was taken successively in the *Z* plane of the biofilm [40 *Z* stacks (*Z* step = 1 m)]. The series of images were 3D-rendered with Leica software and NIH IMAGE processing and analysis in Java freeware. All images were exported as .tif files for digital processing with PHOTOSHOP 6 and ILLUSTRATOR CS2 (Adobe Systems, San Jose, CA).

Plant Infection Assays. Fourteen-day-old sweet corn seedling leaves (*Zea mays* cv. Jubilee; Syngenta, Basel) were inoculated with 10^7 cells of *P. stewartii* strains each expressing the pHC60 plasmid-born GFP_{S65T} gene. The bacterial inoculum was precultured in AB minimal medium supplemented with 0.3% glucose and grown to an OD_{600} of ≈0.3 at 28°C. Cells were harvested and washed with PBS and resuspended in PBS/0.2% Tween 20 to an OD_{600} of 0.3. A 5-μl aliquot of bacterial suspension was deposited into a small incision across a vascular bundle. Plants were incubated in an EGC growth chamber at 28°C daytime, 25°C nighttime, 80% relative humidity, 12-h light [light intensity of 300 $\mu E/m^2$ per s (1E = 1 mol of photons)], and 12-h dark cycle. Bacterial infection and dissemination within intact infected leaves was visualized by fluorescence microscopy 72 h after inoculation. The distance of bacterial dissemination was measured with a ruler. Macroscopic fluorescence images of infected xylem vessels were captured by using a Bio-Rad Laser Molecular Imager FX (FITC fluorophore setting). Leaf tissue and excised xylem vessels were examined by epifluorescence microscopy, performed twice with three replicates for each sample.

Scanning Electron Microscopy. Sweet corn seedlings infected for 12 and 72 h were cross-sectioned to 1-mm thickness on a dental wax pad. Sections were fixed for 3 h with 2.5% glutaraldehyde/2% formaldehyde/0.003 M $MgCl_2$/0.003 M $CaCl_2$/0.05 M Pipes buffer, pH 7. The leaf sections were transferred to 1% aqueous osmium tetroxide solution overnight at room temperature and dehydrated by successive ethanol treatment. Solvents were removed by critical point drying. The samples were mounted onto aluminum stubs, sputter-coated with gold-palladium (1.8 kV and 6 mA for 60 s) and observed by using a Leo/Zeiss DSM 982 digital field emission scanning electron microscope. Scanning electron microscopy analysis was performed twice, with three replicates for each sample.

We thank W. D. Reiter and J. M. Clark, Jr., for critical reading of the manuscript and A. Carlier and C. Herrera for helpful discussions. This work was supported by grants from the National Science Foundation (MCB 0211687), United States Department of Agriculture National Research Initiative Grant 2002-35319-12637, and Cooperative State Research, Education, and Extension Service (CSREES) Grant CONS00775.

1. Fuqua, C. & Greenberg, E. P. (2002) *Nat. Rev. Mol. Cell. Biol.* **35,** 439–468.
2. Kleerebezem, M. & Quadri, L. E. (2001) *Peptides* **22,** 1579–1596.
3. Lazazzera, B. A. (2001) *Peptides* **22,** 1519–1527.
4. Waters, C. M., Antiporta, M. H., Murray, B. E. & Dunny, G. M. (2003) *J. Bacteriol.* **185,** 3613–3623.
5. Whitehead, N. A., Barnard, A. M., Slater, H., Simpson, N. J. & Salmond, G. P. (2001) *FEMS Microbiol. Rev.* **25,** 365–404.
6. Costerton, J. W., Stewart, P. S. & Greenberg, E. P. (1999) *Science* **284,** 1318–1322.
7. Parsek, M. R. & Greenberg, E. P. (2005) *Trends Microbiol.* **13,** 4809–4821.
8. Ramey, B. E., Koutsoudis, M., von Bodman, S. B. & Fuqua, C. (2004) *Curr. Opin. Microbiol.* **7,** 602–609.
9. Stoodley, P., Sauer, K., Davies, D. G. & Coleman, F. (2002) *Annu. Rev. Microbiol.* **56,** 187–209.
10. Kearns, D. B., Chu, F., Branda, S. S., Kolter, R. & Losick, R. (2005) *Mol. Microbiol.* **55,** 739–749.
11. Kaiser, D. (2004) *Annu. Rev. Microbiol.* **58,** 75–98.
12. Viollier, P. H. & Shapiro, L. (2004) *Curr. Opin. Microbiol.* **7,** 572–578.
13. Davies, D. G., Parsek, M. R., Pearson, J. P., Iglewski, B. H., Costerton, J. W. & Greenberg, E. P. (1998) *Science* **280,** 295–298.
14. O'Toole, G. A., Kaplan, H. B. & Kolter, R. (2000) *Annu. Rev. Microbiol.* **54,** 49–79.
15. Webb, S. J., Givskov, M. & Kjelleberg, S. (2003) *Curr. Opin. Microbiol.* **6,** 578–585.
16. Withers, H., Swift, S. & Williams, P. (2001) *Curr. Opin. Microbiol.* **4,** 186–193.
17. Fuqua, C., Winans, S. C. & Greenberg, E. P. (1996) *Annu. Rev. Microbiol.* **50,** 727–751.
18. Waters, C. M. & Bassler, B. L. (2005) *Annu. Rev. Cell. Dev. Biol.* **21,** 319–346.
19. McLean, R. J., Whiteley, M., Stickler, D. J. & Fuqua, W. C. (1997) *FEMS Microbiol. Lett.* **154,** 259–263.
20. Parsek, M. R. & Fuqua, C. (2004) *J. Bacteriol.* **186,** 4427–4440.
21. Parsek, M. R. & Singh, P. K. (2003) *Annu. Rev. Microbiol.* **57,** 677–701.
22. Quiniones, B., Dulla, G. & Lindow, S. E. (2005) *Mol. Plant–Microbe Interact.* **18,** 682–693.
23. Shanks, R. M. Q., Donegan, N. P., Graber, M. L., Buckingham, S. E., Zegans, M. E., Cheung, A. L. & O'Toole, G. A. (2005) *Infect. Immun.* **73,** 4596–4606.
24. Visick, K. L. & McFall-Ngai, M. J. (2000) *J. Bacteriol.* **182,** 1779–1787.
25. Wizniewski-Dye, F. & Downie, J. A. (2002) *Antonie Leeuwenhoek* **81,** 397–407.
26. Crossman, L. & Dow, J. M. (2004) *Microbes Infect.* **6,** 623–629.
27. Daniels, R., Vanderleyden, J. & Michiels, J. (2004) *FEMS Microbiol. Rev.* **28,** 261–289.
28. Huang, J. J., Han, J. I., Zhang, L. H. & Leadbetter, J. R. (2003) *Appl. Environ. Microbiol.* **69,** 5941–5949.
29. Rasmussen, T. B., Bjarnsholt, T., Sindersoe, M. E., Hentzer, M., Kristoffersen, P., Kote, M., Nielsen, J., Eberl, L. & Givskov, M. (2005) *J. Bacteriol.* **187,** 1799–1814.
30. von Bodman, S. B., Majerczak, D. R. & Coplin, D. L. (1998) *Proc. Natl. Acad. Sci. USA* **95,** 7687–7692.
31. Stewart, F. C. (1897) *N.Y. Agric. Exp. Station Bull.* **130,** 422–439.
32. Cook, K. A., Weinzierl, R. A., Pataky, J. K., Esker, P. D. & Nutter, F. W. J. (2005) *J. Econ. Entomol.* **98,** 673–682.
33. Braun, E. J. (1982) *Phytopathology* **72,** 159–166.
34. Leigh, J. A. & Coplin, D. L. (1992) *Annu. Rev. Microbiol.* **46,** 307–346.
35. von Bodman, S. B. & Farrand, S. K. (1995) *J. Bacteriol.* **177,** 5000–5008.
36. Watson, W. T., Minogue, T. D., Val, D. L., Beck von Bodman, S. & Churchill, M. E. A. (2002) *Mol. Cell* **9,** 685–694.
37. Minogue, T. D., Carlier, A. L., Koutsoudis, M. D. & von Bodman, S. B. (2005) *Mol. Microbiol.* **56,** 189–203.
38. Minogue, T. D., Wehland-von Trebra, M., Bernhard, F. & von Bodman, S. B. (2002) *Mol. Microbiol.* **44,** 1625–1635.
39. Dazzo, F. B., Napoli, C. A. & Hubbell, D. H. (1976) *Appl. Environ. Microbiol.* **32,** 166–171.
40. Lippincott, B. B. & Lippincott, J. A. (1969) *J. Bacteriol.* **97,** 620–628.
41. Sequeira, L. (1985) *J. Cell Sci. Suppl.* **2,** 301–316.
42. de Souza, A. A., Takita, M. A., Coletta-Filho, H. D., Caldana, C., Goldman, G. H., Yanai, G. M., Muto, N. H., de Oliveira, R. C., Nunes, L. R. & Machado, M. A. (2003) *Mol. Plant–Microbe Interact.* **16,** 867–875.
43. Guilhabert, M. R. & Kirkpatrick, B. C. (2005) *Mol. Plant–Microbe Interact.* **18,** 856–868.
44. Leite, B., Andersen, P. C. & Ishida, M. L. (2004) *FEMS Microbiol. Lett.* **230,** 283–290.
45. Marques, L. L. R., Ceri, H., Manfio, G. P., Reid, D. M. & Olson, M. E. (2002) *Plant Disease* **86,** 633–638.
46. Meng, Y., Li, Y., Galvani, C. D., Hao, G., Turner, J. N., Burr, T. J. & Hoch, H. C. (2005) *J. Bacteriol.* **187,** 5560–5567.
47. Newman, K. L., Almeida, R. P., Purcell, A. H. & Lindow, S. E. (2004) *Proc. Natl. Acad. Sci. USA* **101,** 1737–1742.
48. Fray, R. G., Throup, J. P., Daykin, M., Wallace, A., Williams, P., Stewart, G. S. & Grierson, D. (1999) *Nat. Biotechnol.* **17,** 1017–1020.
49. Mae, A., Montesano, M., Koiv, V. & Palva, E. T. (2001) *Mol. Plant–Microbe Interact.* **14,** 1035–1042.
50. Scott, R. A., Weil, J., Le, P. T., Williams, P., Fray, R. G., von Bodman, S. B. & Savka, M. A. (2006) *Mol. Plant–Microbe Interact.* **19,** 227–239.
51. Coplin, D. L. & Majerczak, D. (1990) *Mol. Plant–Microbe Interact.* **3,** 286–292.
52. Reeves, P. R., Hobbs, M., Valvano, M. A., Skurnik, M., Whitfield, C., Coplin, D. L., Kido, N., Klena, J., Maskell, D., Raetz, C. R. H. & Rick, P. D. (1996) *Trends Microbiol.* **4,** 495–502.
53. Danese, P. N., Pratt, L. A. & Kolter, R. (2000) *J. Bacteriol.* **182,** 3593–3596.
54. von Bodman, S. B., Ball, J. K., Faini, M. A., Herrera, C. M., Minogue, T. D., Urbanowski, L. M. & Stevens, A. M. (2003) *J. Bacteriol.* **185,** 7001–7007.
55. Bogs, J., Bruchmuller, I., Erbar, C. & Geider, K. (1998) *Phytopathology* **88,** 418–421.
56. O'Toole, G. A. & Kolter, R. (1998) *Mol. Microbiol.* **28,** 449–461.
57. Cheng, H.-P. & Walker, G. C. (1998) *J. Appl. Microbiol.* **180,** 5183–5191.